Mechanical regulation of a molecular clutch defines force transmission and transduction in response to matrix rigidity.

Alberto Elosegui-Artola[1], Roger Oria[1,2], Yunfeng Chen[3,4], Anita Kosmalska[1,2], Carlos Pérez-González[1,2], Natalia Castro[1], Cheng Zhu[3,4,5], Xavier Trepat[1,2,6], Pere Roca-Cusachs[1,2,*].

[1]*Institute for Bioengineering of Catalonia, Barcelona 08028, Spain.*

[2]*University of Barcelona, Barcelona 08028, Spain.*

[3]*Woodruff School of Mechanical Engineering, Georgia Institute of Technology, Atlanta, GA 30332, USA*

[4]*Parker H. Petit Institute for Bioengineering and Bioscience, Georgia Institute of Technology, Atlanta, GA 30332, USA*

[5]*Coulter Department of Biomedical Engineering, Georgia Institute of Technology, Atlanta, GA 30332, USA*

[6]*Institució Catalana de Recerca i Estudis Avançats (ICREA), Barcelona 08010, Spain.*

[*]Author for correspondence:

Pere Roca-Cusachs, PhD

Assistant professor

Institute for Bioengineering of Catalonia / University of Barcelona

C/ Baldiri i Reixac, 15-21, 08028, Barcelona Spain

Tel: (+34) 934 020 863 Email: rocacusachs@ub.edu

Cell function is highly dependent on tissue rigidity, which cells probe by first applying and transmitting forces to their extracellular matrix, and then transducing them into biochemical signals. Here we show that in response to matrix rigidity and density, force transmission and transduction are explained by the mechanical properties of the actin-talin-integrin-fibronectin clutch. We demonstrate that force transmission is regulated by a dynamic clutch mechanism, which only unveils its fundamental biphasic force/rigidity relationship upon talin depletion. Force transduction is then triggered by talin unfolding above a stiffness threshold. Below this threshold, integrins unbind and release force before talin can unfold. Above the threshold, talin unfolds and binds to vinculin, leading to adhesion growth and YAP nuclear translocation. Matrix density, myosin contractility, integrin ligation, and talin mechanical stability differently and non-linearly regulate both force transmission and the transduction threshold. In all cases, coupling of talin unfolding dynamics to a theoretical clutch model quantitatively predicts cell response. Our results establish a molecular mechanism of rigidity sensing spanning from the initial force-induced molecular conformational change to signal relay to the nucleus.

Cell function[1] and major processes in cancer[2] and development[3] are driven by the mechanical rigidity of tissues, which cells probe through their contractile and adhesive molecular machinery. This machinery is composed of dynamic molecular bonds between the extracellular matrix (ECM), integrins, adaptor proteins, and the force-generating actomyosin cytoskeleton, forming a mechanical link generally referred to as a "molecular clutch"[4-6]. To sense and respond to rigidity, cells employ this molecular clutch first to transmit forces to their surrounding matrix[5, 7-9], and then to transduce those forces into biochemical signals leading to transcriptional regulation in the nucleus[10]. The first step of force transmission has been modelled by introducing the dynamic properties of the clutch in computational simulations[4], in a way that can predict the effects of adhesion mediated by different integrin types[5]. However, the fundamental prediction of such clutch model is a biphasic force/rigidity relationship, which is in direct

contradiction with the monotonically increasing curves observed in the vast majority of systems[11-15]. Further, the key molecular clutch elements driving force transmission remain to be identified. The second step of force transduction is likely mediated by force-induced molecular conformational changes, which could occur at the level of ECM molecules, integrins, adaptor proteins, and ion channels, among others[16, 17]. Among all potential mechanosensing molecules, the adaptor protein talin is a particularly interesting candidate since it directly links integrins to actin, is stretched as cells transmit forces to the ECM[18, 19], and mediates cellular response to force[20, 21]. Further, talin has been observed to unfold under force in vitro, exposing previously cryptic binding domains to vinculin[22] which then binds and is likely activated[23]. However, if and how talin unfolding, or conformational changes in any other molecule, mediate rigidity sensing is unknown. Thus, how force transmission and transduction are coupled in response to rigidity remains unresolved.

RESULTS

Talin sets a stiffness threshold that increases force transmission and triggers force transduction.

To understand how rigidity regulates both force transmission and transduction, we used talin 1 -/- mouse embryonic fibroblasts, which have a wild type phenotype due to expression of talin 2[20, 21], and knocked down talin 2 levels using shRNA. We first plated control and talin 2-depleted cells on polyacrylamide gels of different rigidities. The gels were coated with the ECM protein fibronectin, to which cells adhered specifically through α5β1 and αvβ3 integrins (Supplementary Fig. 1). Then, we measured cell-ECM force transmission using traction force microscopy. On the softer substrates, cellular forces increased with rigidity, and talin depletion had no effect (Fig. 1a,b). However, forces sharply diverged above a threshold rigidity of 5 kPa, increasing and decreasing for control cells and depleted cells, respectively (Fig. 1a,b). In control cells, this threshold also coincided with the growth of focal adhesions rich in vinculin (Fig. 1c,d), integrins

and phosphorylated focal adhesion kinase (Supplementary Fig. 2), and with the activation (nuclear translocation) of the mechanosensitive transcriptional regulator YAP[10] (Fig. 1e,f). In contrast, talin-depleted cells spread on the gels, but did not develop focal adhesions or localize YAP to the nucleus at any rigidity (Fig. 1c-f). To confirm those results, we blocked talin function in control cells by mechanism alternative to shRNA. We transfected cells with a dominant negative talin head mutant (L325R) which displaces endogenous talin for integrin binding, but does not activate integrins or link them to the cytoskeleton[24]. On stiff substrates, increasing levels of talin head L325R expression progressively reduced force transmission to the levels of talin depleted cells (Fig. 1g and 1a,b), and abrogated adhesion growth and YAP nuclear translocation as expected (Fig. 1c-f). In contrast and consistently with shRNA results, talin head L325R expression had no effect on soft substrates (Fig. 1g and 1a-f). Those results provide important insights on the two steps required for rigidity sensing, force transmission and force transduction. Regarding force transmission, we show that the core long standing prediction of the clutch adhesion model (a biphasic force/rigidity curve, so far only partially observed in neuronal filopodia[4]) is correct, but only fully unveiled in the absence of talin-mediated reinforcement. Regarding force transduction, we show that it is triggered above a rigidity threshold in a talin-dependent manner, leading to adhesion growth, downstream biochemical signaling, and YAP activation.

Regulation of talin unfolding by a molecular clutch can explain force transmission and transduction in response to rigidity.

We then assessed whether the effects of rigidity and talin could be mediated by known force regulators such as myosin phosphorylation and cell spreading. Whereas myosin phosphorylation levels slightly fluctuated as a function of substrate stiffness and talin depletion (supplementary fig. 3), those fluctuations did not correlate with transmitted forces. Regarding cell spreading

areas, we note that in order to normalize by the possible effect of cell area, all forces reported in figures are already the mean force exerted by cells per unit area. This is also the parameter that directly relates to the output of the model described below. However, to further evaluate the possible role of this parameter we measured cell spreading areas as a function of substrate rigidity and talin depletion (supplementary fig. 3). As reported previously[5], cell areas increased with rigidity, and then reached a plateau at about 5 kPa. However, no significant differences were measured between control and talin-depleted cells. Further, the threshold rigidity between 5 and 11 kPa that led to adhesion growth, YAP activation, and the decrease of forces in talin-depleted cells was not associated with any change in cell spreading area. Thus, neither myosin phosphorylation nor cell spreading could account for the effects of talin, or the rigidity threshold.

Alternatively, the rigidity threshold may result from the regulation of talin unfolding by the ECM-integrin-talin-actin clutch. To investigate this, we compared how force affects the unfolding time of single talin molecules (previously measured[25]) versus the unbinding time of single fibronectin-integrin bonds (both for α5β1 integrins, previously measured[26], and αvβ3 integrins, measured here in Fig. 2a). For clutches mediated by either integrin type, at low forces integrins unbind faster, releasing force transmission and preventing talin unfolding. However, unfolding becomes faster than unbinding above a threshold force (Fig. 2b). This threshold force for unfolding could be further modulated by unbinding events in integrin-talin-actin bonds, which would decrease overall clutch unbinding times, or by load sharing between talin and other adaptor molecules, which would decrease the load on talin and slow unfolding. Independently of its specific value, a force threshold for talin unfolding thus emerges, which may mediate the rigidity threshold observed in Fig. 1.

To evaluate this possibility, we developed a computational approach to couple talin unfolding to a clutch model[5] (see supplementary information for details). This model considers a given

number of myosin motors progressively pulling on an actin fiber, which is bound to a deformable substrate through molecular clutches formed by adaptor proteins (such as talin), integrins, and fibronectin (Fig. 2c). Once the clutches bind according to a given binding rate, fiber contraction deforms the substrate and results in progressive force loading, which is slow or fast on soft or stiff substrates, respectively. This force loading leads to either clutch unbinding or talin unfolding. If talin unfolds, vinculin is assumed to bind, leading to adhesion reinforcement and growth[20] and integrin recruitment. In the absence of talin unfolding integrins are not recruited, but force is still assumed to be transmitted between integrins and actin through other adaptor proteins[27].

If talin unfolding is not considered, we recapitulate the fundamental prediction of the clutch model[4], i.e. a biphasic force/rigidity curve with an optimal rigidity of maximum force transmission (Fig. 2d, blue line). Below the optimal rigidity, force loads so slowly that clutches unbind from the ECM before exerting significant forces. Above the optimal rigidity, force loading is so fast that clutches unbind from the ECM before other clutches have time to bind, reducing cooperativity and decreasing total force transmission. The presence of talin does not affect the curve at low rigidities, where forces are too low to allow unfolding. However, above a rigidity threshold force loading becomes fast enough to allow talin unfolding before integrin unbinding. This leads to vinculin binding and integrin recruitment, which increases integrin binding and force transmission, and eliminates the biphasic relationship (Fig. 2d, red line). In all cases, force transmission resists actin contraction, leading to a negative correlation between force and actin flow (Fig. 2e). The model closely reproduced our force measurements (see Supplementary Table 1 and supplementary information for model parameters and assumptions). Confirming the validity of the clutch hypothesis, actin flows correlated negatively with forces, and could also be reproduced by the model using the same parameters (Fig. 2e,f, and Supplementary Videos 1 and 2). Thus, control of talin unfolding by force transmitted through the ECM-actin clutch can explain how rigidity regulates both force transmission, and the threshold for mechanotransduction.

The rigidity threshold is mediated by talin unfolding under force and subsequent vinculin binding.

We then carried out several experiments to validate this mechanism molecularly. First, we rescued talin 2-depleted cells with either full length (FL) talin 1 or two separate fragments, the talin 1 rod and the talin 1 head. FL talin 1 rescued rescue force generation, adhesion growth, and YAP localization to control levels, confirming that talin 1 and 2 had the same effect[20, 21]. However, neither the talin rod nor the head rescued the phenotype of depleted cells (Fig. 3a-d). Since the talin head is sufficient to activate integrins[21, 28], this shows that integrin activation per se without force transmission through talin was not sufficient to trigger a rigidity response. Further confirming that talin function required an intact mechanical link between engaged integrins and actin, FL talin mutants that either do not bind integrins (W359A) or bind but do not activate integrins (L325R)[24] did not rescue force generation or YAP localization above the rigidity threshold (Fig. 3e,f). Second, we generated a talin mutant (FL talin 1 IVVI) containing 4 point mutations shown to increase the force required for talin unfolding (that is, the force where unfolding rates become faster than refolding rates) from 5 to 8 pN[25]. This should increase the threshold rigidity for unfolding, displacing the effect of talin to higher rigidities. Accordingly, cells rescued with IVVI instead of wild-type talin diverged from talin depleted cells (in terms of force generation, adhesion growth, and YAP translocation) at a higher rigidity (15 instead of 11 kPa) (Fig. 4a-d). This result demonstrates that adhesion growth and YAP activation in response to rigidity are triggered by talin unfolding, and that this response can be regulated by modulating talin mechanical stability.

We then evaluated whether the effect of talin unfolding was mediated by vinculin binding. To this end, we transfected control cells with VD1, a vinculin fragment which is dominant over endogenous vinculin for talin binding[29] but prevents normal vinculin function[30, 31] due to the lack

of remaining functional domains. Blocking vinculin function through VD1 transfection had the same effect than talin depletion, that is, forces decreased at high rigidities, and YAP remained cytosolic (Fig. 4e,f and Supplementary Fig. 4). VD1 formed large focal adhesions above but not below the rigidity threshold (Fig. 4g), confirming that vinculin binding was specifically triggered above the threshold. Since VD1 transfection reduced forces and abrogated YAP signaling above the threshold, those results also show that force transmission rather than adhesion formation per se determines downstream signaling. As a negative control, transfection of a VD1 mutant (A501) with reduced affinity to talin had no effect (Fig. 4e-g). Neither VD1 nor VD1 A501 had any effect on talin-depleted cells (Supplementary Fig. 4). Collectively, those data show that force unfolds talin above a rigidity threshold, leading to vinculin binding, adhesion growth, and YAP translocation to the nucleus.

The molecular determinants of the clutch regulate force transmission and transduction.

Finally, we analyzed the role of different clutch molecular determinants which have been predicted to regulate force transmission[32, 33]. First, if the number of clutches available for binding is decreased (by reducing substrate fibronectin coating density, see supplementary fig. 5), the clutch model predicts that overall force transmission is reduced. However, force loading on each clutch increases because actomyosin contractility is distributed among less clutches, triggering talin unfolding, reinforcement, and YAP translocation at a lower rigidity threshold. Because the rigidity corresponding to peak force transmission in depleted cells is also determined by force loading[32, 33], it also shifts to a lower value. If fibronectin coating is increased, the inverse effect is expected. Second, reducing the binding rate of integrins (by partially blocking integrins with the GPen peptide) should also reduce the number of bound clutches, leading to very similar effects to those of reducing fibronectin coating. However, in this case the reinforcement and adhesion growth triggered upon talin unfolding is impaired because integrins are partially

blocked. This impaired reinforcement counters the effect of the increased loading per integrin. Therefore, the global effect is a reduction in overall force transmission and a shift to lower rigidities of the peak force in depleted cells, but no major change in the threshold rigidity for reinforcement and YAP translocation. Third, decreasing myosin contractility (by using different concentrations of blebbistatin) should reduce force loading, increasing the rigidity threshold required to trigger talin unfolding and YAP activation. Similarly, the force peak in depleted cells should shift to higher rigidities, and reduce its height. All those predictions were verified experimentally (Fig. 5). Although model predictions did not always provide an exact quantitative match, they consistently predicted 1) the shifts in overall forces, 2) the rigidity threshold at which forces diverge for control and depleted cells, and 3) the position of the force peak in depleted cells. Those predictions were obtained by adjusting only the relevant parameters in each case: number of fibronectin molecules (n_f) for fibronectin coating (Fig. 5a,d,g), integrin binding and recruitment rates (k_{ont} and d_{add}) for GPen (Fig. 5b,e,h), and number of myosin motors (n_m) for blebbistatin (Fig. 5c,f,i). In all cases, YAP localized to the nucleus at the same rigidity threshold where measured forces diverged between control and depleted cells (Fig. 5j,k,l). Thus, force transmission was systematically modulated by the molecular determinants of the clutch, leading to mirror shifts in the thresholds for talin unfolding and YAP activation.

DISCUSSION

Our results show that the different properties under force of talin and integrin-fibronectin bonds allow talin unfolding only above a rigidity threshold, leading to vinculin binding, adhesion reinforcement, and YAP signaling. The force/rigidity feedback, and the threshold rigidity for unfolding and YAP translocation, can be tuned according to a quantitative clutch model by modifying talin mechanical properties, ECM coating density, cell contractility, or integrin activity. Our results unveil the mechanisms by which microenvironment rigidity regulates both force transmission and transduction, and reconcile previous findings. Indeed, even though cell-ECM

adhesion is widely accepted to be mediated by a molecular clutch mechanism, its predicted biphasic force/rigidity relationship has been elusive to observe. In most systems, force tends instead to increase monotonically with stiffness, eventually saturating[11-14]. Here we show that the biphasic force/rigidity relationship is normally masked by talin-mediated reinforcement and adhesion growth, and is only fully unveiled upon talin depletion. This depletion allowed us to fully test the molecular determinants of force transmission, revealing that its regulation by rigidity, ECM coating density, cell contractility, or integrin activity fully abides by the clutch model first proposed seven years ago[4, 32, 33]. This leads to interesting and counter-intuitive results, such as that that decreasing ECM coating enhances the mechanical response (fig. 5j), or that mild myosin inhibition (5-15 μM) increases cell-ECM force transmission in talin depleted cells for a specific rigidity range (10-15 kPa, fig. 5c,f). This is because although overall contractility is reduced, the force peak is shifted to higher rigidities. Those results emphasize that mechanical responses cannot be understood merely through individual molecular events, but rather require an integrated and collective view of the mechanochemical network involved.

Whereas in this work we focused on fibronectin substrates bound to cells via α5β1 and αvβ3 mediated catch bonds, we note that the emergence of a threshold for talin unfolding does not require catch bonds per se. Even if talin unfolding and integrin unbinding behaved both as slip bonds, a rigidity threshold would occur simply if the force/unbinding and force/unfolding curves crossed at a given force. Given the extremely steep decay in talin unfolding times as a function of force (fig. 2a), this is likely to happen in a vast majority of scenarios. Further, talin unfolding at low forces would also be prevented by very fast refolding rates, a factor which was also included in our modelling. Thus, the force and rigidity threshold for talin unfolding likely applies in many physiological scenarios, and could be regulated by several factors. First, clutch unbinding events at the level of integrin-talin-actin bonds could increase overall clutch unbinding rates, displacing the threshold to higher forces/rigidities. This effect would alter the specific values of model output, but would not modify the overall trends of the force/rigidity

curves with and without talin, the presence of a rigidity threshold for unfolding, or the regulation of this threshold by the different factors. Second, load sharing between talin and other adaptor proteins could reduce the force experienced by individual talin molecules, also increasing the threshold. Indeed, the best fit of our model was obtained by setting the fraction of force on talin to 7.3% (see table S1), suggesting that talin only experiences a small fraction of the load transmitted by integrins (of the order of a few pN). This is consistent with recently measured tension levels across single talin molecules within cells[18], and with several results both from this work and from the literature. Traction force results show that talin depletion and blocking (Fig. 1) or the IVVI talin mutant with altered mechanical properties (Fig. 3) do not affect force transmission at low rigidities, indicating that other adaptor proteins bear the majority of the load. Such other adaptor proteins may for instance include α-actinin, which we previously reported to transmit a larger share of the load than talin[27]. Additionally, the extremely soft properties of talin[16] imply that it would have to stretch by very long amounts to effectively carry load. The much stiffer properties of other adaptor proteins, such as α-actinin or filamin, suggest that they may be better at this function. Accordingly, the value for clutch spring constant (k_c) that we employed in our modelling is a good fit to the stiffness of filamin or α-actinin but not talin[16]. Collectively, those data support the notion that talin is a soft molecule precisely to allow unfolding at low forces, thereby detecting force levels without impairing force transmission (which would be transmitted through other molecules).

An open question arising from our work is how vinculin binding to talin leads to adhesion growth and YAP translocation. The mechanisms involved likely include talin-induced integrin clustering[34-36], signaling triggered by vinculin activation upon talin binding[37], vinculin-actin binding to reinforce the mechanical clutch[29, 38], and the relay of mechanical forces to the nucleus through stress fibers[39, 40]. Nevertheless and independently of downstream events, our study clarifies how rigidity regulates force transmission, and how force transmission is in turn converted into a biochemical signal. Given the myriad physiological and pathological processes

associated with tissue stiffening[41] and YAP signaling[42], this understanding may also open the door to further fundamental discoveries in biology, and novel therapeutic strategies.

Methods

Cell culture constructs, and transfection. Talin $1^{-/-}$ mouse embryonic fibroblasts were described previously[20, 21], and cultured in DMEM 1x (Life Technologies, 41965), supplemented with 15% FBS. Wild-type Mouse embryonic fibroblasts were also described previously[20], and cultured in DMEM supplemented with 10% FBS. All transfections were carried out using the Neon transfection device according to manufacturer's instructions. To deplete talin levels, cells were transfected with talin 2 shRNA, which contained puromycin resistance (previously described[21]). One day after transfection, cells were incubated with 2 µg/ml puromycin for four days to select for transfected cells. Resulting transfection efficiency was of 52%, with a standard deviation of 11% (see supplementary fig. 3). EGFP-talin1 was a gift of Prof. Crithcley's lab and described previously[43], EGFP-talin1 IVVI was prepared in house from EGFP-talin1 by introducing four point mutations (T809I/T833V/T867V/T901I). EGFP-talin1 head (Addgene plasmid # 32856) and EGFP-talin1 rod (Addgene plasmid # 32855) were obtained from Anna Huttenlocher[44]. EGFP-VD1 (Addgene plasmid # 46270, described as pEGFPC1/GgVcl 1-258) and EGFP-VD1 A501 (Addgene plasmid # 46271, described as pEGFPC1/GgVcl 1-258 A50I) were obtained from Susan Craig[30]. EGFP-FL Talin 1 W359A and EGFP Talin 1 L325R (both FL and head fragment) were gifts of Mark Ginsberg's lab and described previously[24] .Lifeact-GFP was described previously[5]. For Talin 2 shRNA experiments, cells were transfected with Talin 2 shRNA + corresponding plasmid 5 days before experiments. For Control cells, transfections were made the day before experiments.

Antibodies and Chemicals. To block integrin function, we used an inhibitory antibody against α5β1 (10 µg/ml, clone BMB5 produced in rat, Millipore) and a GPen-GRGDSPCA peptide (called GPen throughout the text) specifically recognizing αvβ3 integrin[20, 45] (Bachem). Blebbistatin was from CalBiochem. Antibodies used for immunostaining were a β3 monoclonal antibody recognizing the ligand-bound integrin (clone LIBS1) kindly provided by Mark Ginsberg's lab[46], a vinculin monoclonal antibody (clone h-Vin1 produced in mouse, Sigma), and a rabbit polyclonal

antibody recognizing focal adhesion kinase phosphorylated at tyrosine 397 (Thermofisher). For YAP measurements, we used Hoechst 33342 (Invitrogen) to stain the nucleus and a YAP monoclonal antibody (clone 63.7 produced in mouse, Santa Cruz). Phalloidin-Tetramethylrhodamine B isothiocyanate (Sigma) was used to label actin. For western blots, we used a talin monoclonal antibody (clone 8d4 produced in mouse, Sigma), a Myosin Light Chain polyclonal antibody produced in rabbit (Cell Signaling), a Phospho-Myosin Light Chain polyclonal antibody produced in rabbit (Cell Signaling) and a GAPDH monoclonal antibody (clone 6C5 produced in mouse, Santa Cruz).

Preparation of polyacrylamide gels. Polyacrylamide gels were prepared as previously described[5]. Briefly, glass-bottom dishes (Mattek) were activated with a solution of 3-(Trimethoxysilyl)propyl methacrylate (Sigma), acetic acid and ethanol (1:1:14), washed three times with ethanol and air-dried for 10 min. To generate gels of different stiffness, different concentrations of acrylamide and bis-acrylamide were mixed (see Supplementary Table S2) in a solution containing 0.5% ammonium persulphate, 0.05% tetramethylethylenediamine (Sigma), 0.4% fluorescent red carboxylated nanobeads (Invitrogen), and 4.8 mg/ml NH-acrylate. 10 µl of this solution were then placed on the centre of glass-bottom dishes and covered with 12 mm diameter glass coverslips. After gel polymerization, top coverslips were removed and gels were incubated with fibronectin (Sigma) overnight at 4 ºC. After washing gels with PBS, cells were then trypsinized and plated on gels. Experiments were carried out 4-8 h after cell seeding. To compare fibronectin coating densities on the gels, fibronectin used for coating was previously labelled with an alexa fluor 488 protein labeling kit according to manufacturers instructions (A-10235, Thermo Fisher Scientific). Then, fibronectin coating densities at the gel surface were measured by acquiring epifluorescence images with a 20x objective (N.A.= 0.45), and quantifying resulting fluorescence intensity levels.

Polyacrylamide gel stiffness measurements. The stiffness (Young's modulus) of polyacrylamide gels was measured by AFM as previously described[47]. Briefly, measurements were made with a custom-built AFM attached to an inverted optical microscope (Nikon TE200). Silicon nitride pyramidal tips with an effective half angle θ of 20º and a nominal spring constant of k=0.01-0.03 N/m were used (MLCT, Bruker). The actual spring constant was calibrated by thermal tuning using the simple harmonic oscillator model[48]. The Young´s modulus was measured by recording 10 force-displacement curves with a peak-to-peak amplitude of 6 μm and a frequency of 1 Hz. Three points near the gel centre were selected in each gel, separated 5 μm from each other. For each stiffness, ≥6 gels produced in two batches were measured. To compute the Young´s modulus (E), the Hertz model equation for pyramidal tips was fitted to the force-displacement curves. The equation was fitted for an effective indentation of 1000 nm.

Traction force measurements. Traction force measurements were performed as described previously[5]. Briefly, cells seeded on gels were placed on an inverted microscope (Nikon Eclipse Ti). Phase contrast images of single cells and fluorescence images of the embedded nanobeads were obtained with a 40x objective (N.A. = 0.6). At the end of measurements, cells were trypsinized and an image of bead position in the relaxed state of the gel was acquired. By comparing bead positions with and without cells, a map of gel deformations caused by cells was first obtained using custom particle imaging velocimetry software[49]. Then, after assuming that gel displacements were caused by forces exerted by cells in the cell-gel contact area, the corresponding map of cell forces was calculated using a previously described Fourier transform algorithm[39, 50]. The average forces per unit area exerted by each cell were then calculated. To calculate the minimum detectable force levels for each rigidity, we followed the same procedure in cell-free gel areas, and calculated the resulting forces. Phase contrast images were also used to calculate average cell spreading areas as a function of substrate stiffness.

Immunostaining. For fluorescence staining, cells were fixed with 4% paraformaldehyde, permeabilized with 0.1% Triton X-100, and labelled first with primary antibodies (1 h, room temperature), and then with Alexa-conjugated secondary antibodies (Invitrogen) (1 h, room temperature). Phalloidin was added with the secondary antibody. Fluorescence images were then acquired with a 60x oil immersion objective (NA 1.40) using a spinning disk confocal microscope (Andor). The length of adhesions was assessed by measuring the length of bright vinculin, β3 integri, or pFAK stainings at the cell edge. Integrin density was assessed as described previously[5]. The degree of YAP nuclear localization was assessed by calculating the ratio between YAP fluorescence in the nuclear region and the cytoplasmic region immediately adjacent. Nuclear and cytoplasmic regions were previously determined by co-staining the nucleus with Hoechst 33342.

Rearward flow measurements. To measure actin rearward flow, cells were transfected with lifeact-GFP. Cells were then plated on gels of varying rigidity, and imaged every second for 2 minutes with a 60x oil immersion objective (NA 1.40) with a spinning disk confocal microscope (Andor). For each cell, kymographs were obtained at the cell periphery, and actin speed was measured from the slope of actin features observed in the kymographs. In cells plated on 0.6 kPa gels, actin features were so diffuse that no reliable slopes could be measured in kymographs.

Western blots. For western blotting of Talin, Myosin Light Chain, and Phosphorylated Myosin Light Chain, cells were directly incubated with 1X Laemli and boiled at 95 ºC for 5 minutes. Cell lysates were loaded on 4-20% polyacrylamide gels (Bio-Rad), and electrophoresis proteins were then transferred to a nitrocellulose membrane (Whatman, GE Healthcare Life Sciences), which was blocked with 5% dry-milk-Tris Buffer saline- 0.2% Tween. The membrane was incubated first with primary antibodies (overnight, 4ºC), and then with horseradish peroxidase coupled secondary antibodies (1h, room temperature). Bands were revealed using the LumiLight kit (Roche) and quantified using ImageJ software.

Single fibronectin-αvβ3 bond lifetime measurements. The lifetime of single fibronectin-αvβ3 bonds was measured using a previously described Biomembrane Force Probe (BFP) technique[51]. Biotinylated red blood cells (RBCs) for BFP experiments were collected abiding a Georgia Institute of Technology IRB-approved protocol, and prepared as previously described[51]. Target beads were first covalently linked with anti-Penta His (Histidine) antibody (catalog number 34660, Qiagen, Venlo, Netherlands), and then further covered with Hexa-His tagged recombinant αvβ3 ectodomain, which was a gift from Dr. Junichi Takagi, Osaka University, Japan[52]. Probe beads were first functionalized with streptavidin via covalent linkage and then partially covered with biotinylated fibronectin module III, domain 7-10 ($FN_{III7\text{-}10}$, a generous gift from Dr. Andres Garcia, Georgia Tech). To provide maximum integrin activation, experiments were carried out in the presence of 2 mM Mn^{2+}. In a BFP experiment, the probe bead was glued via biotin-streptavidin interaction onto the apex of the RBC, which was aspirated by a micropipette and acted as a force transducer. A second opposing micropipette grabbed the target bead and drove it to repeatedly impinge the probe bead, contact for 2 sec and then retract (ramping). Displacement of the probe bead was tracked in real-time, which reflected the force exerted on it. If an adhesion event occurred, meaning that one bond or more was formed between the two bead surfaces, ramping resulted in a tensile force signal of the probe bead that pulled on and elongated the RBC. The ramping was then paused at a preset force level (clamping) to wait for bond dissociation, manifested by a backward deformation of the RBC and a sudden force drop to 0 pN. In order to ensure that most adhesion events (>90%) were single molecular interactions, the frequency of adhesion occurrence was adjusted to be low (<20%) by titrating the coating densities on both beads[53]. The time that each adhesion survived during clamping is termed lifetime, which was collected under a range of positive forces. To derive lifetimes under zero-force, the ramping was paused at 0 pN and held for 20 sec. Sudden drops/increases in the thermal fluctuation signal of the probe bead were used to judge the bond association/dissociation, given that bonding suppresses thermal fluctuation[54]. The average

lifetimes were then plotted against the corresponding forces to form a "lifetime vs. force" curve[55]. To confirm binding specificity, control experiments were performed by either adding a αVβ3 blocking antibody (clone LM609, EMD Millipore) or coating beads only with streptavidin instead of $FN_{III7-10}$. Both controls yielded rare binding (~3%).

Statistical analysis. In all figures, measurements are reported as mean ± standard error of the mean (s.e.m). Statistical comparisons were carried out with two-tailed student's t-tests when two cases were compared and with Analysis of variance (ANOVA) tests when more cases were analysed. All tests results are reported in figure legends except in the case of Fig. 5. For all force measurement panels of Fig. 5, differences between control and talin depleted cells were not significant at low rigidities, and started being significant above a stiffness threshold. This threshold was 2, 5, 11 kPa respectively for 1, 10, 100 μg/ml fibronectin coating ($p<0.05$), 5 kPa for all GPen treatments ($p < 0.05$), and 11, 15 kPa respectively for 5, 15 μM blebbistatin treatments ($p < 0.05$). For 50 μM blebbistatin treatment, no significant differences were found at any rigidity. For YAP measurements of Fig. 5, statistical differences were only found in specific cases. For fibronectin coating (fig. 5j), significant differences were found at 5 kPa between 1 μg/ml and both 10 and 100 μg/ml ($p<0.05$). At 11 kPa, significant differences were found between 100 μg/ml and both 1 and 10 μg/ml ($p<0.05$). No statistical differences were found between Gpen treatments (Fig. 5k). For blebbistatin treatments (Fig. 5l), statistical differences were found between 5 μM and, both 15 and 50 μM above 11 kPa ($p<0.05$). Due to space limitations, sample numbers are given as ranges in figure legends. Detailed statistical information on sample numbers and experimental repeats can be found in supplementary table 3.

Code availability. Matlab code employed to generate numerical simulations (see methods for details) is available upon request to rocacusachs@ub.edu.

References

1. Moore, S.W., Roca-Cusachs, P. & Sheetz, M.P. Stretchy proteins on stretchy substrates: the important elements of integrin-mediated rigidity sensing. *Dev.Cell* **19**, 194-206 (2010).
2. Paszek, M.J. *et al.* Tensional homeostasis and the malignant phenotype. *Cancer Cell* **8**, 241-254 (2005).
3. Engler, A.J., Sen, S., Sweeney, H.L. & Discher, D.E. Matrix elasticity directs stem cell lineage specification. *Cell* **126**, 677-689 (2006).
4. Chan, C.E. & Odde, D.J. Traction dynamics of filopodia on compliant substrates. *Science* **322**, 1687-1691 (2008).
5. Elosegui-Artola, A. *et al.* Rigidity sensing and adaptation through regulation of integrin types. *Nat. Mater.* **13**, 631-637 (2014).
6. Case, L.B. & Waterman, C.M. Integration of actin dynamics and cell adhesion by a three-dimensional, mechanosensitive molecular clutch. *Nat. Cell Biol.* (2015).
7. Plotnikov, S.V., Pasapera, A.M., Sabass, B. & Waterman, C.M. Force fluctuations within focal adhesions mediate ECM-rigidity sensing to guide directed cell migration. *Cell* **151**, 1513-1527 (2012).
8. Gupta, M. *et al.* Adaptive rheology and ordering of cell cytoskeleton govern matrix rigidity sensing. *Nature communications* **6**, 7525 (2015).
9. Oakes, P.W., Banerjee, S., Marchetti, M.C. & Gardel, M.L. Geometry regulates traction stresses in adherent cells. *Biophys. J.* **107**, 825-833 (2014).
10. Dupont, S. *et al.* Role of YAP/TAZ in mechanotransduction. *Nature* **474**, 179-183 (2011).
11. Ghibaudo, M. *et al.* Traction forces and rigidity sensing regulate cell functions. *Soft Matter* **4**, 1836-1843 (2008).
12. Schiller, H.B. *et al.* beta1- and alphav-class integrins cooperate to regulate myosin II during rigidity sensing of fibronectin-based microenvironments. *Nat. Cell Biol.* **15**, 625-636 (2013).
13. Ghassemi, S. *et al.* Cells test substrate rigidity by local contractions on sub-micrometer pillars. *PNAS* **109**, 5328-5333 (2012).
14. Califano, J.P. & Reinhart-King, C.A. Substrate Stiffness and Cell Area Predict Cellular Traction Stresses in Single Cells and Cells in Contact. *Cellular and molecular bioengineering* **3**, 68-75 (2010).
15. Etienne, J. *et al.* Cells as liquid motors: mechanosensitivity emerges from collective dynamics of actomyosin cortex. *PNAS* **112**, 2740-2745 (2015).
16. Roca-Cusachs, P., Iskratsch, T. & Sheetz, M.P. Finding the weakest link - exploring integrin-mediated mechanical molecular pathways. *J.Cell Sci.* **125**, 3025-3038 (2012).
17. Schoen, I., Pruitt, B.L. & Vogel, V. The Yin-Yang of Rigidity Sensing: How Forces and Mechanical Properties Regulate the Cellular Response to Materials. *Annual Review of Materials Research* **43**, 589-618 (2013).
18. Austen, K. *et al.* Extracellular rigidity sensing by talin isoform-specific mechanical linkages. *Nat. Cell Biol.* **17**, 1597-1606 (2015).
19. Margadant, F. *et al.* Mechanotransduction in Vivo by Repeated Talin Stretch-Relaxation Events Depends Upon Vinculin. *PLoS Biol.* **9**, e1001223 (2011).
20. Roca-Cusachs, P., Gauthier, N.C., del Rio, A. & Sheetz, M.P. Clustering of $\alpha5\beta1$ integrins determines adhesion strength whereas $\alpha v\beta3$ and talin enable mechanotransduction. *PNAS* **106**, 16245-16250 (2009).
21. Zhang, X. *et al.* Talin depletion reveals independence of initial cell spreading from integrin activation and traction. *Nat. Cell Biol.* **10**, 1062-1068 (2008).
22. del Rio, A. *et al.* Stretching Single Talin Rod Molecules Activates Vinculin Binding. *Science* **323**, 638-641 (2009).

23. Chen, H., Choudhury, D.M. & Craig, S.W. Coincidence of actin filaments and talin is required to activate vinculin. *J. Biol. Chem.* **281**, 40389-40398 (2006).
24. Wegener, K.L. *et al.* Structural Basis of Integrin Activation by Talin. *Cell* **128**, 171-182 (2007).
25. Yao, M. *et al.* Mechanical activation of vinculin binding to talin locks talin in an unfolded conformation. *Scientific reports* **4**, 4610 (2014).
26. Kong, F., Garcia, A.J., Mould, A.P., Humphries, M.J. & Zhu, C. Demonstration of catch bonds between an integrin and its ligand. *J. Cell Biol.* **185**, 1275-1284 (2009).
27. Roca-Cusachs, P. *et al.* Integrin-dependent force transmission to the extracellular matrix by alpha-actinin triggers adhesion maturation. *PNAS* **110**, E1361-E1370 (2013).
28. Tanentzapf, G. & Brown, N.H. An interaction between integrin and the talin FERM domain mediates integrin activation but not linkage to the cytoskeleton. *Nat. Cell Biol.* **8**, 601-606 (2006).
29. Hirata, H., Tatsumi, H., Lim, C.T. & Sokabe, M. Force-dependent vinculin binding to talin in live cells: a crucial step in anchoring the actin cytoskeleton to focal adhesions. *Am. J. Physiol. Cell Physiol.* **306**, C607-620 (2014).
30. Cohen, D.M., Kutscher, B., Chen, H., Murphy, D.B. & Craig, S.W. A conformational switch in vinculin drives formation and dynamics of a talin-vinculin complex at focal adhesions. *J. Biol. Chem.* **281**, 16006-16015 (2006).
31. Humphries, J.D. *et al.* Vinculin controls focal adhesion formation by direct interactions with talin and actin. *J. Cell Biol.* **179**, 1043-1057 (2007).
32. Bangasser, B.L., Rosenfeld, S.S. & Odde, D.J. Determinants of maximal force transmission in a motor-clutch model of cell traction in a compliant microenvironment. *Biophys. J.* **105**, 581-592 (2013).
33. Bangasser, B.L. & Odde, D.J. Master equation-based analysis of a motor-clutch model for cell traction force. *Cellular and molecular bioengineering* **6**, 449-459 (2013).
34. Saltel, F. *et al.* New PI(4,5)P2- and membrane proximal integrin-binding motifs in the talin head control beta3-integrin clustering. *J. Cell Biol.* **187**, 715-731 (2009).
35. Klapholz, B. *et al.* Alternative mechanisms for talin to mediate integrin function. *Curr. Biol.* **25**, 847-857 (2015).
36. Iwamoto, D.V. & Calderwood, D.A. Regulation of integrin-mediated adhesions. *Curr. Opin. Cell Biol.* **36**, 41-47 (2015).
37. Case, L.B. *et al.* Molecular mechanism of vinculin activation and nanoscale spatial organization in focal adhesions. *Nat. Cell Biol.* **17**, 880-892 (2015).
38. Thievessen, I. *et al.* Vinculin-actin interaction couples actin retrograde flow to focal adhesions, but is dispensable for focal adhesion growth. *J. Cell Biol.* **202**, 163-177 (2013).
39. Roca-Cusachs, P. *et al.* Micropatterning of single endothelial cell shape reveals a tight coupling between nuclear volume in G1 and proliferation. *Biophys. J.* **94**, 4984-4995 (2008).
40. Swift, J. *et al.* Nuclear lamin-A scales with tissue stiffness and enhances matrix-directed differentiation. *Science* **341**, 1240104 (2013).
41. DuFort, C.C., Paszek, M.J. & Weaver, V.M. Balancing forces: architectural control of mechanotransduction. *Nat. Rev. Mol. Cell Biol.* **12**, 308-319 (2011).
42. Plouffe, S.W., Hong, A.W. & Guan, K.L. Disease implications of the Hippo/YAP pathway. *Trends Mol. Med.* **21**, 212-222 (2015).
43. Bate, N. *et al.* Talin contains a C-terminal calpain2 cleavage site important in focal adhesion dynamics. *PLoS One* **7**, e34461 (2012).
44. Simonson, W.T., Franco, S.J. & Huttenlocher, A. Talin1 regulates TCR-mediated LFA-1 function. *J. Immunol.* **177**, 7707-7714 (2006).
45. Pierschbacher, M.D. & Ruoslahti, E. Influence of Stereochemistry of the Sequence Arg-Gly-Asp-Xaa on Binding-Specificity in Cell-Adhesion. *J. Biol. Chem.* **262**, 17294-17298 (1987).

46. Frelinger, A.L., 3rd, Du, X.P., Plow, E.F. & Ginsberg, M.H. Monoclonal antibodies to ligand-occupied conformers of integrin alpha IIb beta 3 (glycoprotein IIb-IIIa) alter receptor affinity, specificity, and function. *J. Biol. Chem.* **266**, 17106-17111 (1991).
47. Alcaraz, J. *et al.* Microrheology of Human Lung Epithelial Cells Measured by Atomic Force Microscopy. *Biophys. J.* **84**, 2071-2079 (2003).
48. Hutter, J.L. & Bechhoefer, J. Calibration of Atomic-Force Microscope Tips. *Review of Scientific Instruments* **64**, 1868-1873 (1993).
49. Serra-Picamal, X. *et al.* Mechanical waves during tissue expansion. *Nat. Phys.* **8**, 628-U666 (2012).
50. Butler, J.P., Tolic-Norrelykke, I.M., Fabry, B. & Fredberg, J.J. Traction fields, moments, and strain energy that cells exert on their surroundings. *Am.J.Physiol.Cell Physiol.* **282**, C595-C605 (2002).
51. Chen, Y. *et al.* Fluorescence Biomembrane Force Probe: Concurrent Quantitation of Receptor-ligand Kinetics and Binding-induced Intracellular Signaling on a Single Cell. e52975 (2015).
52. Takagi, J., Petre, B.M., Walz, T. & Springer, T.A. Global conformational rearrangements in integrin extracellular domains in outside-in and inside-out signaling. *Cell* **110**, 599-611 (2002).
53. Chesla, S.E., Selvaraj, P. & Zhu, C. Measuring two-dimensional receptor-ligand binding kinetics by micropipette. *Biophys. J.* **75**, 1553-1572 (1998).
54. Chen, W., Zarnitsyna, V.I., Sarangapani, K.K., Huang, J. & Zhu, C. Measuring Receptor-Ligand Binding Kinetics on Cell Surfaces: From Adhesion Frequency to Thermal Fluctuation Methods. *Cellular and molecular bioengineering* **1**, 276-288 (2008).
55. Chen, W., Lou, J. & Zhu, C. Forcing switch from short- to intermediate- and long-lived states of the alphaA domain generates LFA-1/ICAM-1 catch bonds. *J. Biol. Chem.* **285**, 35967-35978 (2010).

Acknowledgements. We acknowledge support from the Spanish Ministry for Economy and Competitiveness (BFU2011-23111 and BFU2012-38146), a Career Integration Grant within the seventh European Community Framework Programme (PCIG10-GA-2011-303848), the European Research Council (Grant Agreements 242993 and 240487), the Generalitat de Catalunya, Fundació La Caixa, and Fundació la Marató de TV3 (project 20133330). A.E.A., R.O., and C.P-G. were supported respectively by a Juan de la Cierva Fellowship (Spanish Ministry of Eonomy and Competitiveness), a FI fellowship (Generalitat de Catalunya), and the fundació "La Caixa". We thank R. Sunyer, J. Alcaraz, E. Bazellières, F. Rico, S. Garcia-Manyes, and the members of the P.R-C. and X.T. laboratories for technical assistance and discussions.

Author contributions. A.E.A. and P.R-C. conceived the study, A.E.A., C.Z, X.T., and P.R-C. designed the experiments, A.E.A., R.O., Y.C., A.J.K., C.P-G., and N.C. performed the experiments, P.R-C. carried out the theoretical modelling, and A.E.A. and P.R.C. wrote the paper.

Author information. The authors declare no competing financial interests. Correspondence and requests for materials should be addressed to rocacusachs@ub.edu.

Figure legends

Figure 1: Talin sets a rigidity threshold that triggers increased force transmission, adhesion maturation and YAP nuclear translocation**. a,** Average forces (n ≥ 10 cells per condition) exerted by control (red) Talin 2 shRNA (blue) and control + Talin 1 Head L325R (white diamond) cells plated on FN-coated polyacrylamide gels of increasing rigidity. In grey, background noise levels show the minimum detectable force for each rigidity value (see methods). Solid line is a fit to experimental results. **b,** Colour maps showing the traction forces applied by example cells in the different conditions plated on 5 and 29 kPa gels. **c,** Quantification of vinculin adhesion length (n≥33 adhesions from ≥7 cells) for the same conditions as in **a**. Lines are sigmoidal fits to experimental results. **d,** Examples of vinculin adhesions on cells plated on 5 and 29 kPa gels. Zoomed regions (10 x 6 μm) correspond to rectangles marked in red in the main image. **e**, Quantification of nuclear/cytosolic YAP ratio (n ≥ 20 cells) for the same conditions as in a). Lines are sigmoidal fits to experimental results. **f,** Examples of YAP staining on cells plated on 5 and 29 kPa gels. In all quantifications (**a,c,e**) differences between control and both talin-depleted and control + Talin 1 Head L325R cells were significant only above 5 kPa ($p<0.05$). Scale bar is 20 μm. Gray dotted line in panels **a,c,e** marks the rigidity threshold. **g**, For control cells, traction forces exerted on 5 kPa gels (blue) and 29 kPa gels (red) as a function of the efficiency of transfection with Talin1 Head L325R. Values are compared to mean forces of untransfected control cells (left) and talin shRNA cells (right). Note that in all other panels, Talin 1 Head L325R data represent averages for well transfected cells only. Dotted lines represent sigmoidal fits to the data.

Figure 2: The balance between clutch unbinding and talin unfolding predicts the force/rigidity curves and the rigidity threshold for mechanotransduction**. a,** Measured average lifetime of fibronectin-αvβ3 bonds as a function of force (red points). Blue line shows previously measured average unfolding times of talin[25]. The threshold force enabling talin unfolding is shown in gray. **b,** Cartoon depicting how force leads to integrin unbinding below the threshold, but talin unfolding above. **c,** Molecular clutch model of force transmission. Myosin motors pull with a speed *v* on actin filaments, which are connected to a compliant substrate (represented as a linear elastic spring of varying rigidity) through several parallel molecular clutches. Once clutches bind to the substrate (with a binding rate k_{on}) force is loaded progressively as the fiber retracts, determining the unbinding rate k_{off} and the unfolding/refolding rates k_{unfold}/k_{fold} according to the profiles in a) (see methods). **d,** Experimental force data from fig. 1a are shown superimposed to model predictions with/without talin unfolding (solid red and blue lines, respectively). Grey line shows the minimum detection level. **e,** Quantification of actin flow speeds (n ≥ 19 traces from ≥ 10 cells) and model predictions (solid lines) for control (red) and Talin 2 shRNA (blue) cells plated on FN-coated polyacrylamide gels of increasing rigidity. **f,** Examples of control and Talin 2 shRNA cells transfected with lifeact-GFP and plated on 5 and 29kPa gels. Insets are kymographs showing the movement of actin features along the lines marked in red. The slope of the traces created by the features (marked with dashed lines) was used to calculate actin speed. Scale bar is 20 μm in main images, and 20 s/2 μm (X/Y axes) in the kymographs.

Figure 3: The rigidity threshold requires an intact integrin-cytoskeletal link mediated by full length talin. **a-c,** average forces (a, n ≥ 10 cells per condition), Nuclear/cytosolic YAP ratios (b, n ≥ 20 cells per condition), and vinculin adhesion lengths (c, n≥41 adhesions from ≥8 cells per

condition) for talin 2 shRNA cells plated on fibronectin-coated gels of increasing rigidity and co-transfected with FL Talin 1, Talin 1 Rod, and Talin 1 Head. Significant differences between FL talin and the other two plasmids were found for forces, YAP ratios, and adhesion lengths only above 5 kPa ($p<0.05$). **d**, Examples of vinculin stainings for cells plated on gels with different rigidities for the conditions indicated. Scale bar is 20 µm. Insets are 10 x 6 µm. **e,** Quantification of traction forces exerted on substrates of 5 kPa and 29 kPa by talin 2 shRNA cells (gray) and talin 2 shRNA cells co-transfected with EGFP-FL Talin 1 (red), EGFP-FL Talin 1 L325R (blue), and EGFP-FL Talin 1 W359A (black) ($n \geq 10$ cells per condition). **f,** Quantification of Nuclear / Cytosolic YAP ratio for the same conditions ($n \geq 10$ cells per condition). Significant differences were observed between Talin 2 shRNA + EGFP-FL Talin 1 and all other conditions at 29 kPa but not 5 kPa (***, $p<0.001$).

Figure 4: The rigidity threshold is mediated by talin unfolding under force and subsequent vinculin binding. **a-c,** average forces (a, $n \geq 10$ cells per condition), Nuclear/cytosolic YAP ratios (b, $n \geq 20$ cells per condition), and vinculin adhesion lengths (c, $n \geq 41$ adhesions from ≥ 8 cells per condition) exerted on fibronectin-coated gels of increasing rigidity by talin 2 shRNA cells or talin 2 shRNA cells co-transfected with FL Talin 1 or FL talin 1 IVVI. Significant differences between Fl talin and FL talin IVVI were found at 11 kPa for all measurements ($p<0.05$). **d,** Examples of vinculin stainings for cells plated on gels with different rigidities for the conditions indicated. **e,f**, average forces (e, $n \geq 10$ cells per condition) and Nuclear/cytosolic YAP ratios (f, $n \geq 20$ cells per condition), exerted on fibronectin-coated gels of increasing rigidity by control cells transfected with EGFP-VD1 or EGFP-VD1 A501. Significant differences between VD1 and VD1 A501 transfection were found for all measurements above 11 kPa but not below ($p<0.05$). **g**, examples of VD1 and VD1 A501 fluorescence distribution for cells plated on gels with different rigidity for the conditions indicated. Scale bar is 20 µm. Insets are 10 x 6 µm.

Figure 5: The elements of the molecular clutch tune force transmission and the rigidity threshold required for talin unfolding and YAP nuclear translocation. **a-d-g,** Average cell traction forces on gels of varying concentration of fibronectin coating. Solid and dotted lines show model predictions with and without talin unfolding, respectively, after adjusting the parameter n_f (number of fibronectin molecules). **a,** 1 µg/ml, n_f=750 **(d)** 10 µg/ml, n_f=1200 (blue, reference condition from fig. 1) and **(g)** 100 µg/ml, n_f=1650 ($n \geq 10$ cells per condition)**., b-e-h,** Same quantification for cells with different concentrations of the integrin blocking peptide GPen. The parameters adjusted were k_{ont} (true integrin binding rate) and d_{add} (number of integrins added after each reinforcement step). **(b)** 0.05 mM, $k_{ont}=1.9\cdot10^{-4}$ µm^2/s, $d_{add}=24$, **(e)** 0.15 mM, $k_{ont}=1.5\cdot10^{-4}$ µm^2/s, $d_{add}=10$, **(h)** 0.50 mM, $k_{ont}=0.9\cdot10^{-4}$ µm^2/s, $d_{add}=6$ ($n \geq 10$ cells per condition). **c-f-i,** Same quantification for cells with different concentrations of the myosin inhibitor blebbistatin. The parameter adjusted was n_m (number of myosin motors) **(c)** 5 µM, n_m=500 **(f)** 15 µM, n_m=300 and **(i)** 50 µM, n_m=180 ($n \geq 10$ cells per condition). Dotted vertical blue lines show the position of the rigidity threshold in reference conditions (no treatment, 10 µg/ml fibronectin coating). In all force quantifications, the grey lines show the minimum detectable force level, which increased with rigidity and reached the values measured for talin-depleted cells at high rigidities. Thus, those values reflect the detection level rather than actual generated forces, which were likely below the detection threshold. **j-k-l,** Quantification of the Nuclear/Cytosolic YAP ratio for control cells in the three different concentrations of **(j)** fibronectin, **(k)** GPEN and

(l) blebbistatin (n ≥ 20 cells per condition). Blue lines show YAP activation levels in reference conditions, other lines are sigmoidal fits to experimental results. See Supplementary Methods for statistical analysis.

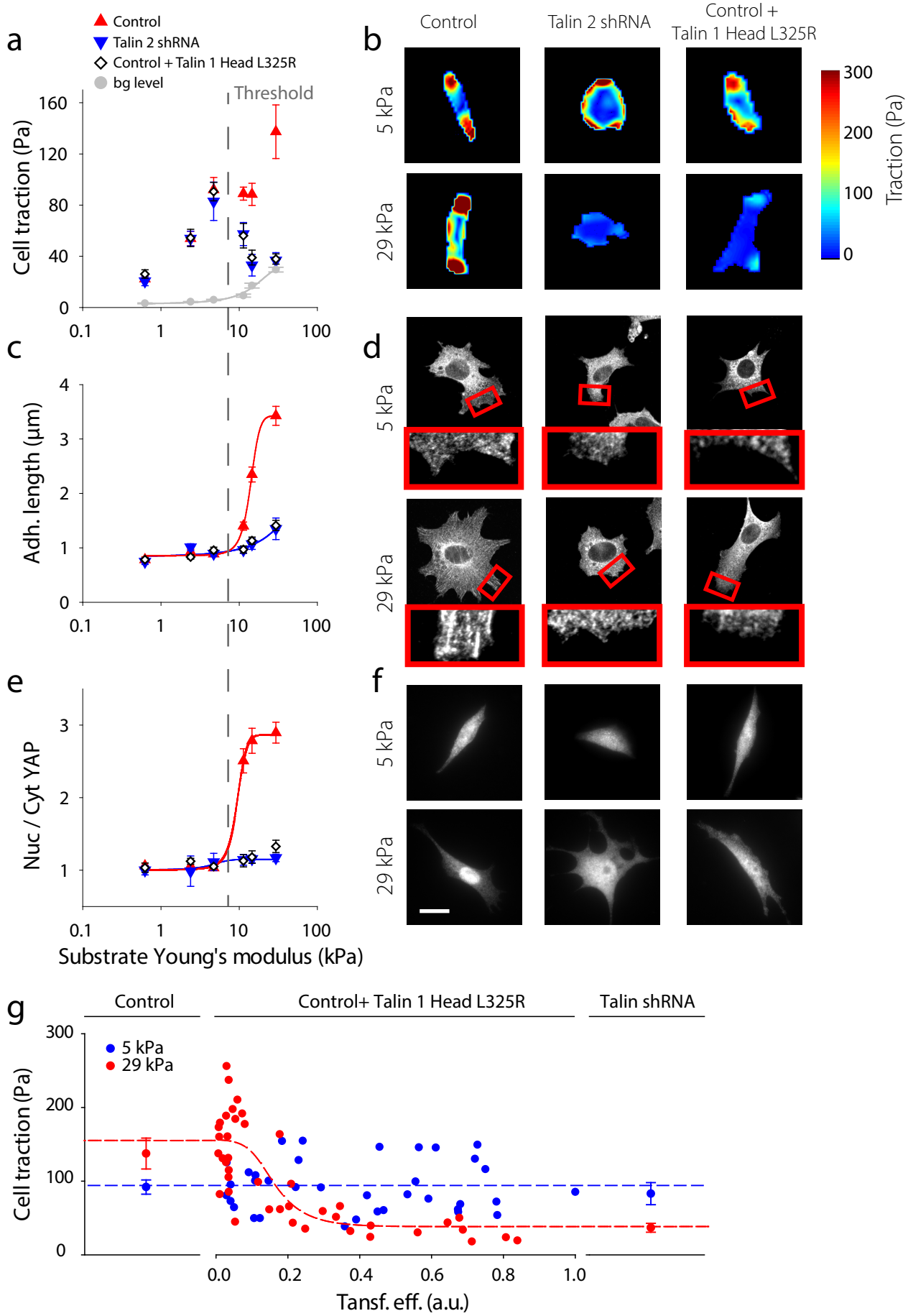
a
Control
Talin 2 shRNA
Control + Talin 1 Head L325R
bg level
Threshold
Cell traction (Pa)
160
120
80
40
0
0.1
1
10
100
b
Control
Talin 2 shRNA
Control +
Talin 1 Head L325R
5 kPa
29 kPa
300
200
100
0
Traction (Pa)
c
Adh. length (µm)
4
3
2
1
0
d
e
Nuc / Cyt YAP
3
2
1
Substrate Young's modulus (kPa)
f
g
Control
Control+ Talin 1 Head L325R
Talin shRNA
5 kPa
29 kPa
Cell traction (Pa)
300
200
100
0
0.0
0.2
0.4
0.6
0.8
1.0
Tansf. eff. (a.u.)

Figure 1

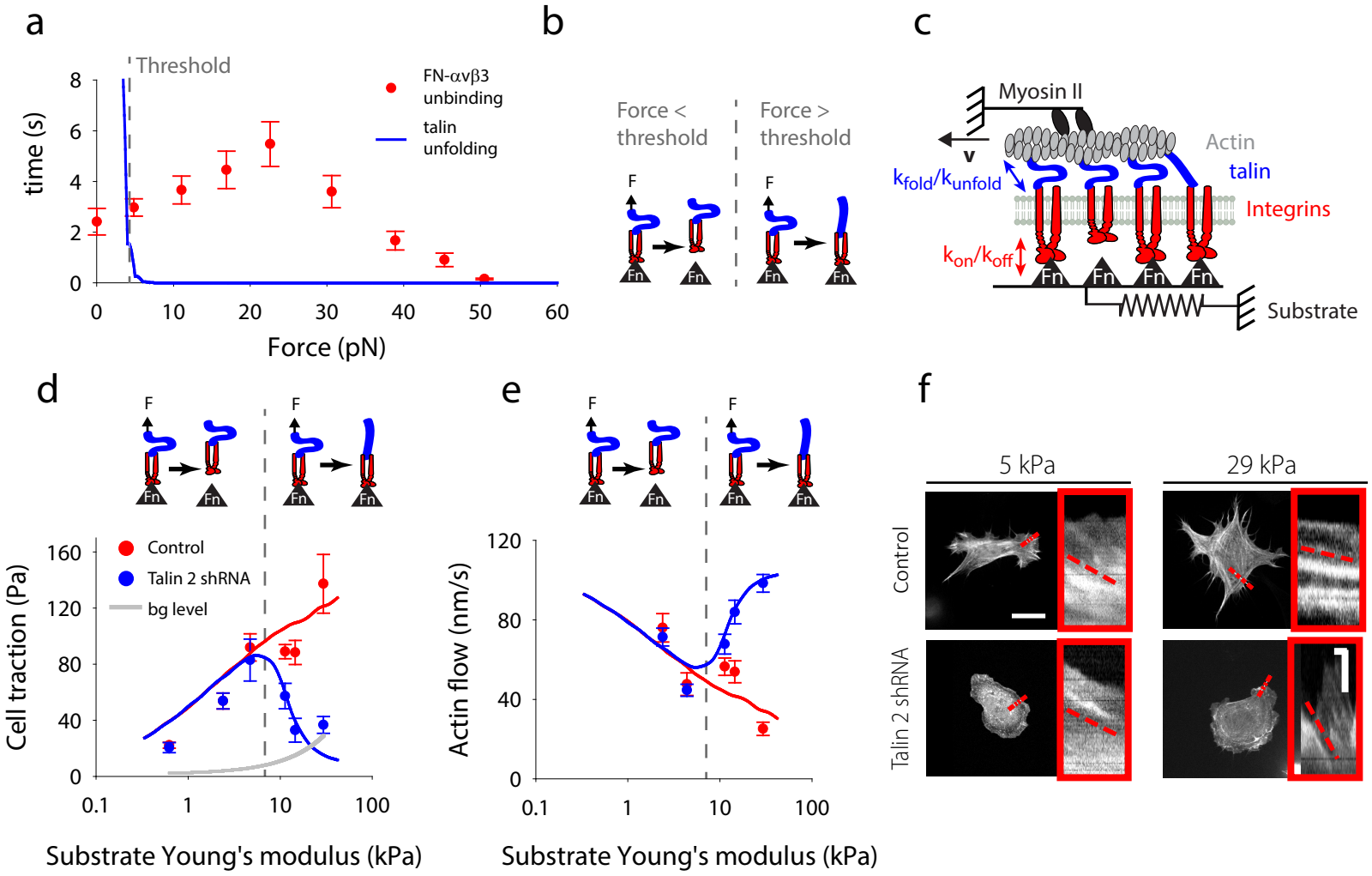
a
Threshold
FN-αvβ3 unbinding
talin unfolding
time (s)
Force (pN)
b
Force < threshold
Force > threshold
F
Fn
c
Myosin II
v
Actin
talin
Integrins
Substrate
kfold/kunfold
kon/koff
d
Control
Talin 2 shRNA
bg level
Cell traction (Pa)
Substrate Young's modulus (kPa)
e
Actin flow (nm/s)
Substrate Young's modulus (kPa)
f
5 kPa
29 kPa
Control
Talin 2 shRNA

Figure 2

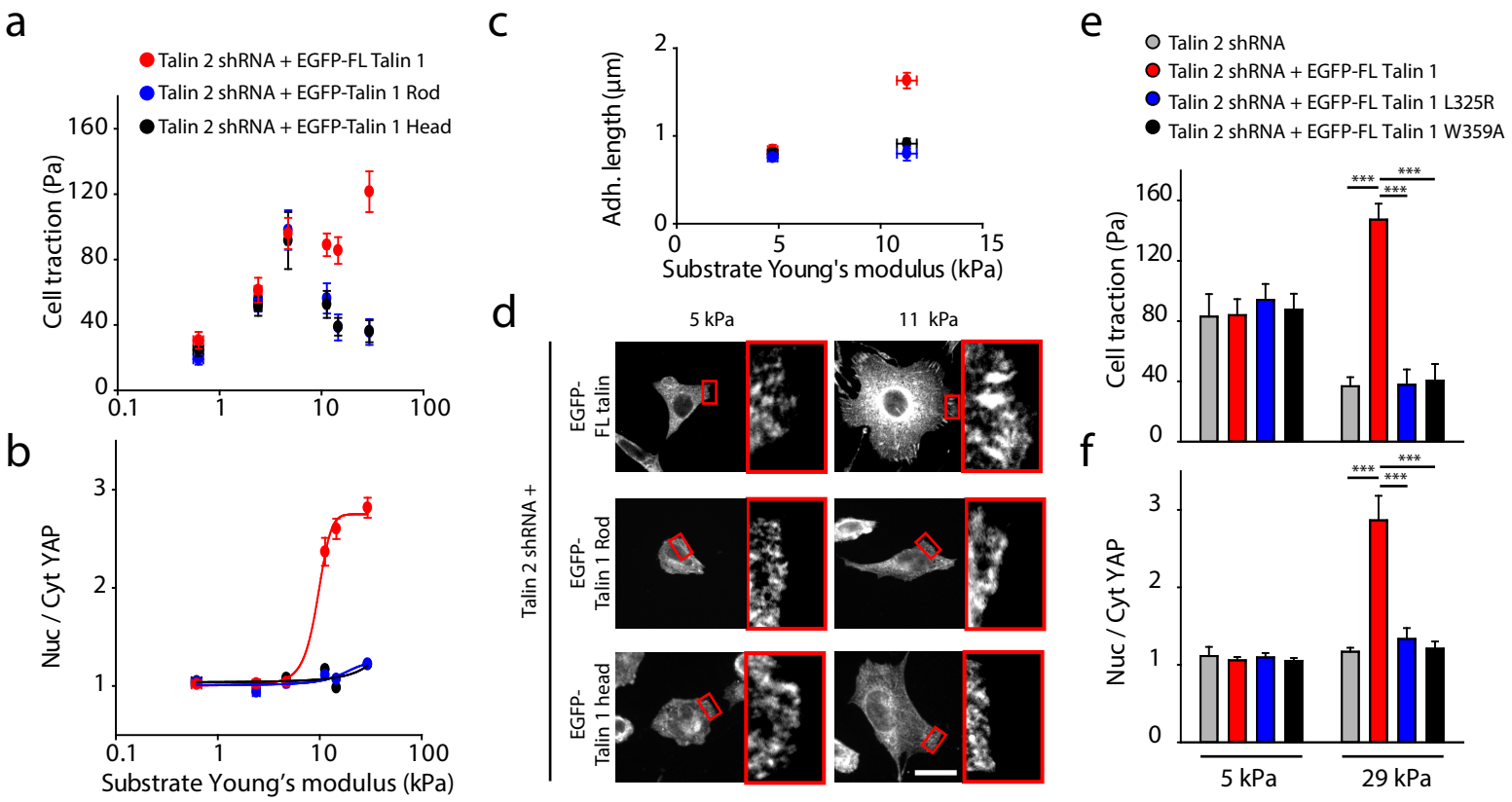
a
Talin 2 shRNA + EGFP-FL Talin 1
Talin 2 shRNA + EGFP-Talin 1 Rod
Talin 2 shRNA + EGFP-Talin 1 Head
Cell traction (Pa)
160
120
80
40
0
0.1
1
10
100
b
Nuc / Cyt YAP
3
2
1
0.1
1
10
100
Substrate Young's modulus (kPa)
c
Adh. length (μm)
2
1
0
0
5
10
15
Substrate Young's modulus (kPa)
d
5 kPa
11 kPa
Talin 2 shRNA +
EGFP-FL talin
EGFP-Talin 1 Rod
EGFP-Talin 1 head
e
Talin 2 shRNA
Talin 2 shRNA + EGFP-FL Talin 1
Talin 2 shRNA + EGFP-FL Talin 1 L325R
Talin 2 shRNA + EGFP-FL Talin 1 W359A
Cell traction (Pa)
160
120
80
40
0
***
***
***
f
Nuc / Cyt YAP
3
2
1
0
***
***
***
5 kPa
29 kPa

Figure 3

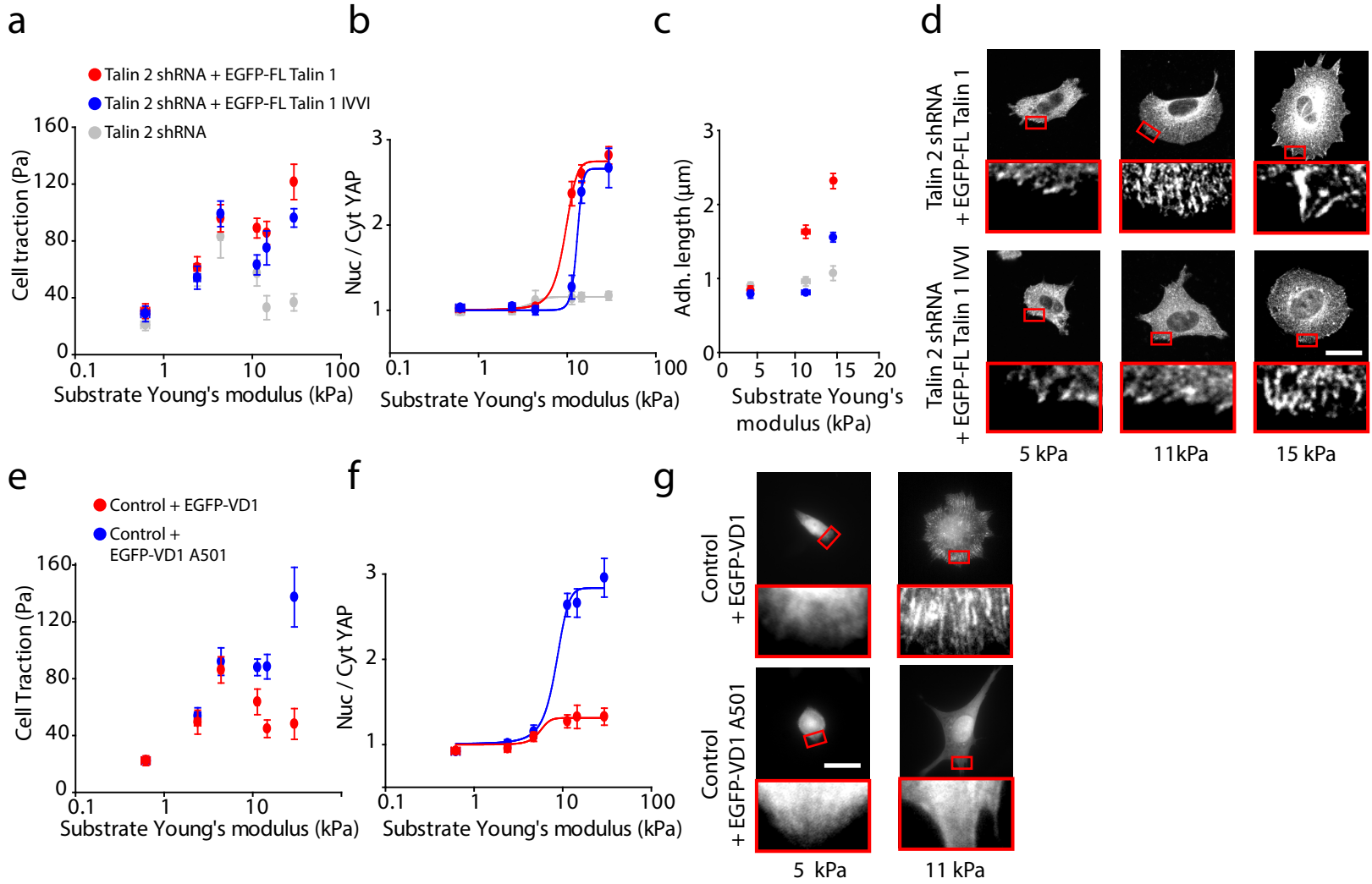
a
b
c
d
Talin 2 shRNA + EGFP-FL Talin 1
Talin 2 shRNA + EGFP-FL Talin 1 IVVI
Talin 2 shRNA
Cell traction (Pa)
Substrate Young's modulus (kPa)
Nuc / Cyt YAP
Substrate Young's modulus (kPa)
Adh. length (µm)
Substrate Young's modulus (kPa)
Talin 2 shRNA + EGFP-FL Talin 1
Talin 2 shRNA + EGFP-FL Talin 1 IVVI
5 kPa
11kPa
15 kPa
e
f
g
Control + EGFP-VD1
Control + EGFP-VD1 A501
Cell Traction (Pa)
Substrate Young's modulus (kPa)
Nuc / Cyt YAP
Substrate Young's modulus (kPa)
Control + EGFP-VD1
Control + EGFP-VD1 A501
5 kPa
11 kPa

Figure 4

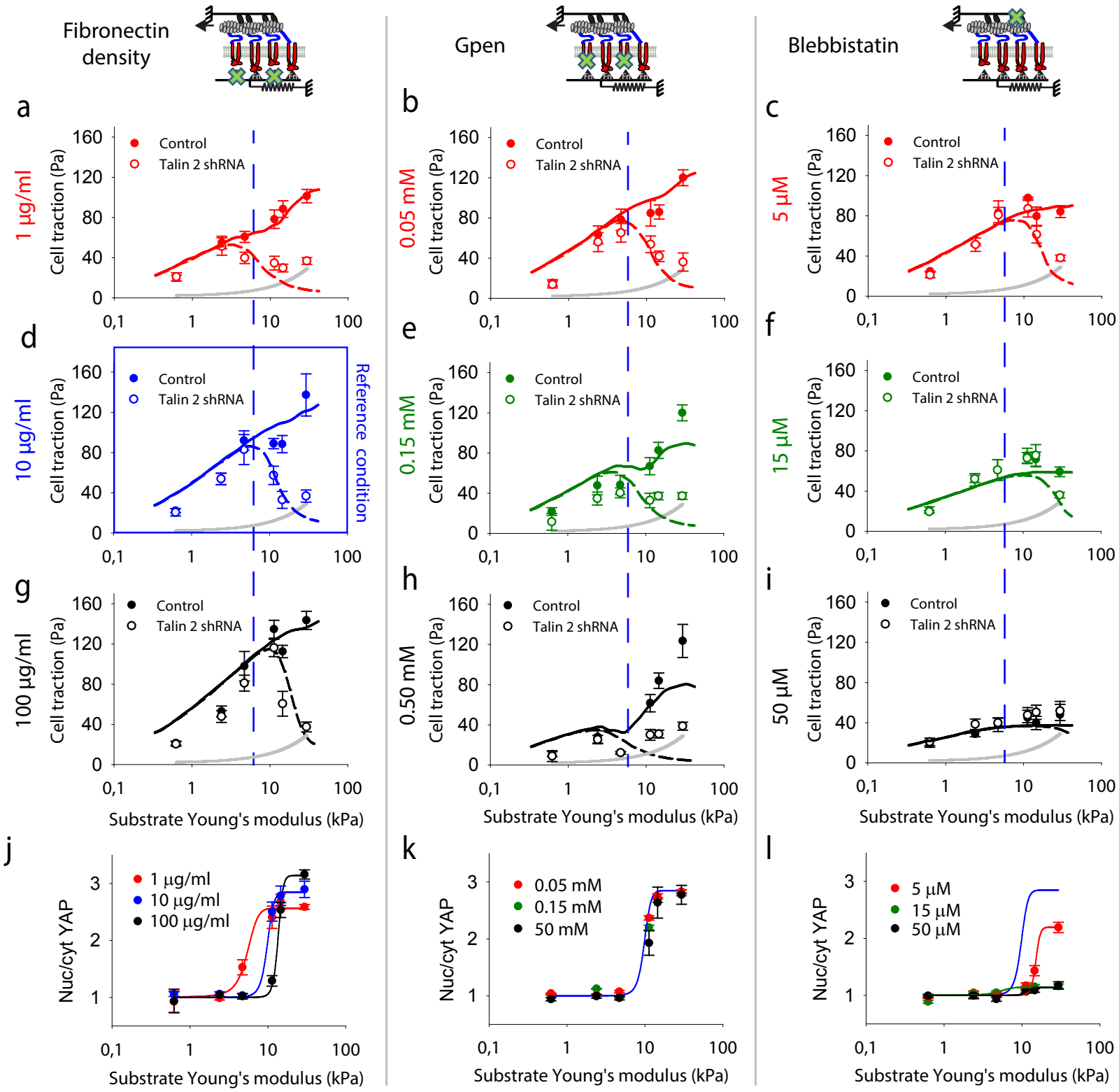
Fibronectin density
Gpen
Blebbistatin
a
b
c
d
e
f
g
h
i
j
k
l
1 µg/ml
10 µg/ml
100 µg/ml
0.05 mM
0.15 mM
0.50 mM
5 µM
15 µM
50 µM
Control
Talin 2 shRNA
Reference condition
Cell traction (Pa)
Substrate Young's modulus (kPa)
Nuc/cyt YAP
0,1
1
10
100
0
40
80
120
160
1
2
3

Figure 5